The sensitivity of landfast sea ice to atmospheric forcing in single-column model simulations: a case study at Zhongshan Station, Antarctica

Fengguan Gu[1], Qinghua Yang[1], Frank Kauker[2,3], Changwei Liu[1], Guanghua Hao[4], Chaoyuan Yang[1], Jiping Liu[5], Petra Heil[6], Xuewei Li[1], Bo Han[1*]

1 School of Atmospheric Sciences, Sun Yat-sen University, and Southern Marine Science and Engineering Guangdong Laboratory (Zhuhai), Zhuhai 519082, China

2 Alfred Wegener Institute, Helmholtz Centre for Polar and Marine Research, Am Handelshafen 12, 27570 Bremerhaven, Germany

3 Ocean Atmosphere Systems, Tewesstseg 4, 20249 Hamburg, Germany

4 Key Laboratory of Marine Hazards Forecasting, National Marine Environmental Forecasting Center, Ministry of Natural Resources, Beijing 100081, China

5 Department of Atmospheric and Environmental Sciences, State University of New York at Albany, Albany, NY, USA

6 Australian Antarctic Division and Australian Antarctic Program Partnership, Private Bag 80, Hobart, Tas 7001, Australia

Correspondence to: Bo Han (hanb5@mail.sysu.edu.cn)

Abstract

Single-column sea ice models are used to focus on the thermodynamic evolution of the ice. Generally these models are forced by atmospheric reanalysis in absence of atmospheric *in situ* observations. Here we assess the sea ice thickness (SIT) simulated by a single-column model (ICEPACK) with *in situ* observations obtained off Zhongshan Station for the austral winter of 2016. In the reanalysis the surface air temperature is about 1 ℃ lower, the total precipitation is about 2 mm day^{-1} larger, and the surface wind speed is about 2 m s^{-1} higher compared to the *in situ* observations, respectively. Using sensitivity experiments we evaluate the simulation bias in sea ice thickness due to the uncertainty in the individual atmospheric forcing variables. We show that the unrealistic precipitation in the reanalysis leads to a bias of 14.5 cm in sea ice thickness and of 17.3 cm in snow depth. In addition, our data show that increasing snow depth works to gradually inhibits

the growth of sea ice associated with thermal blanketing by the snow due to changing the vertical heat flux. Conversely, given suitable conditions, the sea ice thickness may grow suddenly when the snow load gives rise to flooding and leads to snow-ice formation. A potential mechanism to explain the different characteristics of the precipitation bias on snow and sea ice is discussed. The flooding process for landfast sea ice might cause different effect compared to pack ice, thus need to be reconsidered in ICEPACK. Meanwhile, the overestimation in surface wind speed in reanalysis is likely responsible for the underestimation in simulated snow depth, however this had little influence on the modelled ice thickness.

1 Introduction

Sea ice plays an important role in the global climate system by reflecting solar radiation and regulating the heat, moisture and gas exchanges between the ocean and the atmosphere. In contrast to the rapid decline of sea ice extent and volume in the Arctic (Stroeve et al., 2012; Lindsay and Schweiger, 2015), satellite observations show a slight increase in the yearly-mean area of Antarctic sea ice since the late 1970s (Parkinson and Cavalieri, 2012) followed by a rapid decline from 2014 (Parkinson, 2019) and a renewed increase in most recent years (Chemke and Polvani, 2020). Although the sudden decline of Antarctic sea ice is yet to be attributed (Parkinson, 2019), the spatial pattern of Antarctic sea ice changes is suggested to be largely caused by changes in the atmospheric forcing. For example, the rapid ice retreat in the Weddell Sea from 2015 to 2017 has been associated with the intensification of northerly wind (Turner et al., 2017), while the phase of the southern annular mode (SAM) significantly modulates the sea ice in Ross Sea and elsewhere, especially in November 2016 (Stuecker et al., 2017; Schlosser et al., 2018; Wang et al., 2019a).

Landfast sea ice, the immobile fraction of the sea ice, is mainly located in near coastal regions of Antarctica and its change is assumed to be indicative for the evolution of total Antarctic sea ice (Heil et al., 1996; Heil, 2006; Lei et al., 2010; Yang et al., 2016a). Different from drifting sea ice, the change in landfast sea ice is dominated by thermodynamic processes which can be simulated by single-column sea ice models (Heil et al., 1996; Lei et al., 2010; Yang et al., 2016b; Zhao et al., 2017). Furthermore, a single-column sea ice model is a useful tool to evaluate the impacts of different atmospheric forcings on the sea ice evolution because of the relatively simple structure of the physical processes (Cheng et al., 2013; Wang et al., 2019b; Merkouriadi et al., 2020). In this

study, a state of the art single-column sea ice model, ICEPACK, is chosen to investigate the sensitivity of landfast sea ice to atmospheric forcing for the region off Zhongshan Station in Prydz Bay, East Antarctica (Figure 1).

Due to the lack of *in situ* observation, the majority of sea ice studies, especially for the Antarctic, rely on numerical models. Realistic atmospheric forcing is critical for reliable model simulations. Although being criticized for large deviations from *in situ* observations (Bromwich et al., 2007; Vancoppenolle et al., 2011; Wang et al., 2016; Barthélemy et al., 2018), atmospheric reanalysis data are assumed to offer reasonable atmospheric forcing for large-scale sea ice models for the Antarctic (Zhang, 2007; Massonnet et al., 2011; Zhang, 2014; Barthélemy et al., 2018). Previous studies reported a large spread between four global atmospheric reanalysis products and *in situ* observations in the Amundsen Sea Embayment (Jones et al., 2016). Moreover, studies showed that directly using atmospheric reanalysis as forcing for models causes significant biases in the Arctic sea ice simulations (Lindsay et al., 2014; Wang et al., 2019b). Similar results, accentuated by the sparseness at atmospheric observations entering the reanalysis, can be foreseen for Antarctica. Therefore, before simulating Antarctic sea ice the atmospheric forcing needs to be evaluated carefully. To our knowledge, few studies have given a quantitative evaluation on the effect of different atmospheric forcing on sea ice simulations in Antarctica.

The coastal landfast sea ice in Prydz Bay is generally first-year ice. It usually fractures and is exported or melts out completely between December and the following February and refreeze occurs from late February onwards (Lei et al., 2010). This seasonal cycle is representative of Antarctic landfast sea ice. In this study, we are aiming to evaluate the contributions of the various atmospheric forcing variables on landfast sea ice growth. The snow cover exerts influence on evolution of the vertical sea ice-snow column via a number of mechanisms, including the formation of snow-ice added by flooding (Leppäranta, 1983), superimposed ice (Kawamura et al., 1997) and insulating impact (Massom et al., 2001). Understanding the snow depth is a major concern here.

Two sets of atmospheric forcing have been chosen. The first is spatially interpolated ERA5 onto the location of the observation site, and the second is using in situ atmospheric observations. It is well-known that the simulation biases of numerical models are introduced through many shortcomings including unrealistic surface boundary conditions (here: atmospheric forcing), imperfect physical process formulations, computational errors. Understanding the uncertainty in sea

ice simulations as well as the sea ice response pattern to atmospheric forcing due to imperfect surface boundaries is a prerequisite for successful simulations and needs to be assessed first.

This study is arranged as follow: In section 2 the employed *in situ* observations, the numerical model and the reanalysis are introduced. The main results are given in section 3 focusing on the effect of different kinds of atmospheric forcing on sea ice and snow. Discussion and conclusions follow in sections 4 and 5.

2 Materials and methods

2.1 Meteorological observations

The site of sea ice observation is in the coastal area off Zhongshan Station [(69◦22′S,76◦22′E); Figure 1], East Antarctica. The meteorological data were collected at a year-round manned weather observatory run at Zhongshan Station in 2016, which is 1 km inland from the sea ice observation site and 15 m above sea level. Snow fall is measured every 12 hours at the Russian Progress II station (located ~1 km to the southeast of Zhongshan Station). The short- and long-wave radiation were measured every minute with a net radiometer mounted 1.5 m above the surface on a tripod (Yang et al., 2016a). Other meteorological variables are available as hourly data, including 2 m air temperature (T_{2m}), surface pressure (P_a), specific humidity (calculated from dew-point temperature and P_a), potential temperature (calculated from T_{2m} and P_a), air density (calculated by T_{2m} and P_a) and 10 m wind speed (U_{10}) (Hao et al., 2019; Hao et al., 2020; Liu et al., 2020).

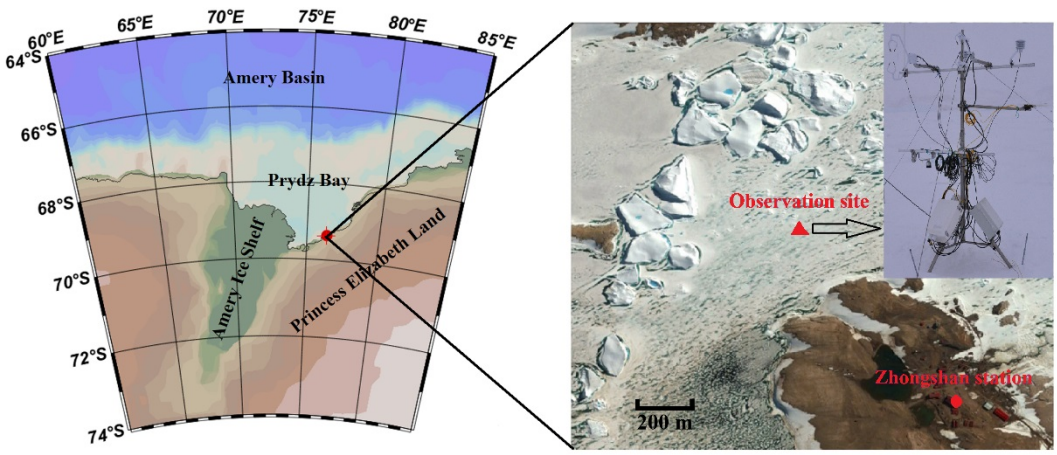

Figure 1 Location of landfast sea ice surface measurements near Zhongshan Station. The solid triangle denotes the observation site, the solid circle marks Zhongshan Station.

2.2 Sea ice thickness measurement

A thermistor-chain unit developed by Taiyuan University of Technology (TY) was used to measure sea ice thickness in austral winter 2016. This unit is composed of two parts: the control unit and the thermistor chain. The controller initiates data acquisitions, and records and stores the temperature measurements. The thermistor chain is 3 m long with 250 equidistant thermistors. Their sensitivity is 0.063 ℃, and the measurement accuracy is better than ±0.5 ℃. The thermistor chain records the vertical temperature profile across the near-surface atmosphere, any snow cover, the sea ice and the surface sea water simultaneously. Measurements are hourly. Details about the instruments are given in Hao et al. (2019).

Snow thickness close to the thermistor unit is measured weekly using a ruler with an accuracy of ±0.2 cm. Sea ice thickness is measured with ruler through a drill hole (5 cm diameter) weekly, the measurement accuracy is ±0.5 cm. The average thickness obtained from three close-by sites is retained. The measurement accuracy of ice thickness is ±0.5 cm. Sea-surface temperature and sea-surface salinity are measured in the drill holes weekly using a Cond 3210 set 1 (Hao et al., 2019).

2.3 Atmospheric reanalysis data

The European Centre for Medium-range Weather Forecasts (ECMWF) released ERA5, the new reanalysis product in 2017 which is updated in near real-time (Hersbach and Dee, 2016; Hersbach et al., 2020). The complete ERA5 dataset, extending back to 1950, has been available to the end of 2019 during this study. Compared with the popular ERA-Interim reanalysis there are several major improvements in ERA5, including much higher resolutions (both, spatially and temporally). ERA5 has global coverage with a horizontal resolution of 31 km by 31 km at the equator and 10 km by 31 km at the latitude of Zhongshan Station. In the vertical ERA5 resolves the atmosphere using 137 vertical pressure levels from the surface up to a geopotential height of 0.01 hPa. ERA5 provides hourly analysis and forecast fields and applies a four dimensional variational data assimilation system (4D-var). Data frequency is daily. ERA5 includes various reprocessed quality-controlled data sets, for example, the reprocessed version of the Ocean and Sea Ice Satellite Application Facilities (OSI SAF) sea ice concentration (Hersbach and Dee, 2016; Hersbach et al., 2020). For comparison and evaluation against observations in the Antarctic, ERA5 is bilinearly interpolated with 4 surrounding grid points to the observation site (described in 2.1).

2.4 ICEPACK

ICEPACK is a column-physics component of the Los Alamos Sea Ice Model (CICE) V6 and is maintained by the CICE Consortium. ICEPACK incorporates column-based physical processes that affect the area and thickness of sea ice. It includes several options for simulating sea ice thermodynamics, mechanical redistribution (ridging) and associated area and thickness changes. In addition, the model supports several tracers, including thickness, enthalpy, ice age, first-year ice area, deformed ice area and volume, melt ponds, and biogeochemistry (Hunke et al., 2019). ICEPACK Version 1.1.1 was used in this study and detailed options of physical parameterizations and model settings for the ICEPACK are summarized in Table 1. We employ ICEPACK to distribute the initial ice thickness to each ice thickness category using a distribution function:

$$p_i = \frac{max\left(2 \times h \times H_i - H_i^2, 0\right)}{\sum max\left(2 \times h \times H_i - H_i^2, 0\right)}, i = 1, N$$

Where, h is initial ice thickness, H_i is the prescribed ice thickness category (0–0.6, 0.6–1.4, 1.4–2.4, 2.4–3.6, and above 3.6 m~; same as for Arctic simulations), N is the number of ice thickness categories.

Table 1 Detailed options of physical parameterizations and model settings for the ICEPACK.

ICEPACK	**Value**
time step	3600 s
Number of layers in the ice	7
Number of layers in the snow	1
Ice thickness categories	5 (Bitz et al., 2001)
Initial ice thickness	99.5 cm (observed)
Initial snow depth	11.5 cm (observed)
Albedo scheme	CCSM3 (Collins et al., 2006)
Ice thermodynamic	Mushy-layer (Turner et al., 2013)
Shortwave radiation	Delta-Eddington (Briegleb and Light, 2007)
Snowdrift	Not implemented in ICEPACK 1.1.1
Melt ponds (superimposed ice)	Not used in this study

The atmospheric forcing for the ICEPACK model consists of observations of downward short- and longwave radiation, 2 m air temperature, specific humidity, total precipitation, potential temperature, 2 m air density, and 10 m wind speed. The oceanic forcing includes sea surface temperature, sea surface salinity, and oceanic mixed layer depth. The period concerned in this study

is from 22 April, when observed sea ice generally starts to grow, to 22 November in 2016. Since there are no observations of the ocean mixed-layer depth, we set it to 10 m based on a previously published study (Zhao et al., 2019).

3 Results

3.1 Surface atmospheric conditions near the observation site

First we compare the eight atmospheric variables used to force ICEPACK (surface downward shortwave radiation (R_{sd}), surface downward longwave radiation (R_{ld}), surface air temperature (T_a), specific humidity (Q_a), precipitation (P), air potential temperature (Θ_a), air density (ρ_a), wind speed (U_a) with the respective *in situ* observation. Table 2 lists the bias (simulation minus observation), bias ratio (ratio between the bias and the observation value), the mean value of the *in situ* observation (Mean_Obs), the correlation coefficient (Corr.) and the root-mean-square deviation (RMSD) between the interpolated ERA5 data and the observation. In general, all eight variables from the two sources follow each other quite closely (correlation coefficients between ERA5 and the observations greater than 0.85), except for P and U_a. In this study, the main attention is on the atmospheric variables T_a, P, and U_a for three reasons: (1) Previous studies have shown that from all atmospheric forcing variables, uncertainties in T_a, P, and U_a exert significantly impact on the sea ice thickness (Cheng et al., 2008). (2) surface wind may affect the snow cover in two ways: a) sublimation strongly reduces the snow cover in dry air and strong wind condition (Gascoin et al., 2013), b) surface wind modulates the latent and sensible heat fluxes in the bulk formation (Fairall et al., 2003). (3) P and U_a from the reanalysis have the largest bias ratio compared to the *in situ* observations.

The timing of daily variations of T_a are well represented by ERA5, especially for strong cooling events (Figure 2a). However, ERA5 tends to underestimate warm events by a few degree as well as cold events where differences exceeding 10 ℃ may occur (Figure 2d). During the entire observation period in 2016, T_a from ERA5 was 1.168 ℃ lower than in the *in situ* observation. Also previous studies reported similar disagreement in T_a between observation and reanalysis in Antarctica (Bracegirdle and Marshall, 2012; Fréville et al., 2014). The cold bias of T_a in the reanalysis was suggested to be caused by the ice surface schemes that cannot accurately describe the ice-atmosphere interactions of strongly stable stratified boundary layers that are frequent in Antarctica.

Table 2 Comparison of atmospheric forcing between ERA5 reanalysis and *in situ* observations.

Variable	Bias	Bias ratio (%)	Mean_Obs	Corr	RMSD
R_{sd} (W m^{-2})	6.115	9.031	67.714	0.967	40.981
R_{ld} (W m^{-2})	-19.153	-9.672	198.023	0.869	28.753
T_a (K)	-1.168	-0.453	257.809	0.967	2.820
Q_a (10^{-4} kg kg^{-1})	-0.769	-9.326	8.247	0.950	1.987
P (mm day^{-1})	2.010	303.509	0.660	0.639	0.825
Θ_a (K)	0.290	0.112	259.437	0.965	2.609
ρ_a (kg m^{-3})	-0.021	-1.592	1.322	0.958	0.026
U_a (m s^{-1})	2.145	50.735	4.228	0.765	2.989

The reanalyzed variable with the largest bias ratio from the observation is the precipitation (Figure 2b). Hourly precipitation from ERA5 was accumulated into daily data and compared with the daily precipitation records from the Progress II station. The maximum daily mean precipitation can reach 19.1 mm day^{-1} (11 July 2016) with an average precipitation of 0.66 mm day^{-1} from April 29 to November 22, 2016. While ERA5 captures the main precipitation events, it significantly overestimated the magnitude of precipitation events, especially in July. In this month, the mean precipitation rate from ERA5 is 5.83 mm day^{-1}, while observed is only 1.42 mm day^{-1}. From April to November, the accumulated precipitation from ERA5 is about 300% larger than that in the *in situ* observations. Nevertheless, using precipitation from Progress II for Zhongshan Station may be questioned as well because of the distance of about 1 km to Zhongshan Station. Moreover, strong wind causes snow drift events and the precipitation observation might not collect all snow fall correctly. This may cause larger bias between ERA5 and observations during strong events.

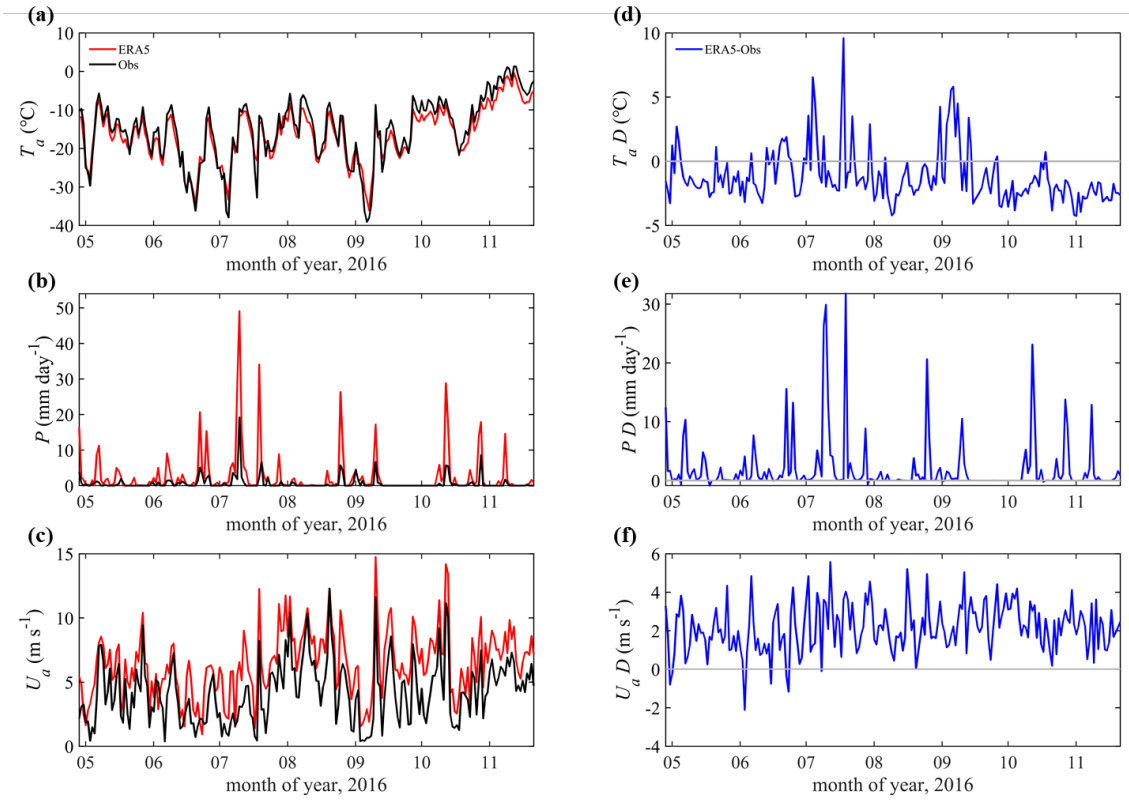

Figure 2 Time series of daily (a) surface air temperature, (b) precipitation rate, and (c) wind speed (10 m above the surface). The ERA5 reanalysis data are indicated as red lines. Observations are marked by black lines. (d-f) show the difference (marked by '*D*') between ERA5 and the observation (ERA5-observation). The differences are marked by blue lines. The gray lines denote the zero line.

The wind speed observation varied from 0.01 m s^{-1} to 12.3 m s^{-1} with an average 4.2 m s^{-1} and with maxima in August (Figure 2c). ERA5 well captured the timing of strong wind events but overestimated the magnitude of daily surface wind on average by 2.1 m s^{-1}. One potential cause of the overestimation is that the numerical model underlying ERA5 cannot represent the roughness correctly due to the complex orography (Tetzner et al., 2019) and the effect of katabatic wind regions (Vignon et al., 2019).

3.2 Simulation forced by observed *in situ* atmospheric variables

The simulation bias of sea ice thickness and snow depth is impacted by many aspects, including unrealistic atmospheric and oceanic forcing and shortcomings in the applied numerical model. In this study, we mainly focus on the influence of imperfect atmospheric forcing.

The sea ice thickness (Obs) measured through a hole drilled is increasing from 29 April (100±2

cm) to 25 October (172±2 cm), remaining level from there on (Figure 3a). The ice thickness deduced from the TY (Obs_TY) thermistor-chain buoy shows a similar result: sea ice thickness increasing from 106 cm on 22 April to 171 cm on 17 November. In November the sea ice thickness (Obs and Obs_TY) is stationary, indicating a thermodynamic equilibrium between heat loss to the atmosphere and heat gain from the ocean (Yang et al., 2016a; Hao et al., 2019).

When forced by atmospheric *in situ* observations, the simulated sea ice thickness (Sim_Obs) agrees well with the observed thickness with a mean bias of less than 1 cm over the growth season. We attribute the good simulation result to the fact that seasonal evolution of landfast is largely driven by thermal processes which ICEPACK captures well using *in situ* forcing.

The average Obs snow depth during the ice-growth season is 17 cm with low snow depth measured prior to 11 July (Figure 3b). Thereafter, the snow depth increases rapidly up to about 37 cm associated with a precipitation event arising from a single synoptic system. Then it decreases below the seasonal mean (Obs_mean) followed by two secondary maxima in exceeding the seasonal mean (about 25 cm) on 8 September and 18 October.

The Sim_Obs snow depth tracks the observation closely before 2 August (Figure 3b). Then, the Obs snow depth decreased quickly from about 30 cm to about 10 cm, while the Sim_Obs snow depth continues to increase gradually until the onset of surface melting in November. We attribute the Obs quick decrease of snow depth to the effect of snowdrift, because the surface wind stayed above 5 m s^{-1} for most of August (Figure 2c), giving rise to snow drift, a process not implemented in the version of ICEPACK used here. In addition, Sim_Obs snow depth cannot capture the magnitude of Obs on 11 July. As discussed above, using precipitation from Progress II for Zhongshan Station could be questioned. Moreover, a given precipitation rate (snow fall) might cause a wide range of snow cover patterns because the snowdrift is quite strong and responsible for larger deviation in snow depth between Sim_Obs and Obs (Liston et al., 2018).

Using observed meteorological variables as atmospheric forcing in ICEPACK produce unreliable snow depth while the sea ice thickness was in reasonably good agreement. In other words, the large bias in snow depth seems to have little effect on the sea ice thickness in the simulation. This counter-intuitive finding is of great interest to us because the snow layer is crucial in modulating the energy exchange on top of the sea ice. Potential causes of for this result will be discussed later.

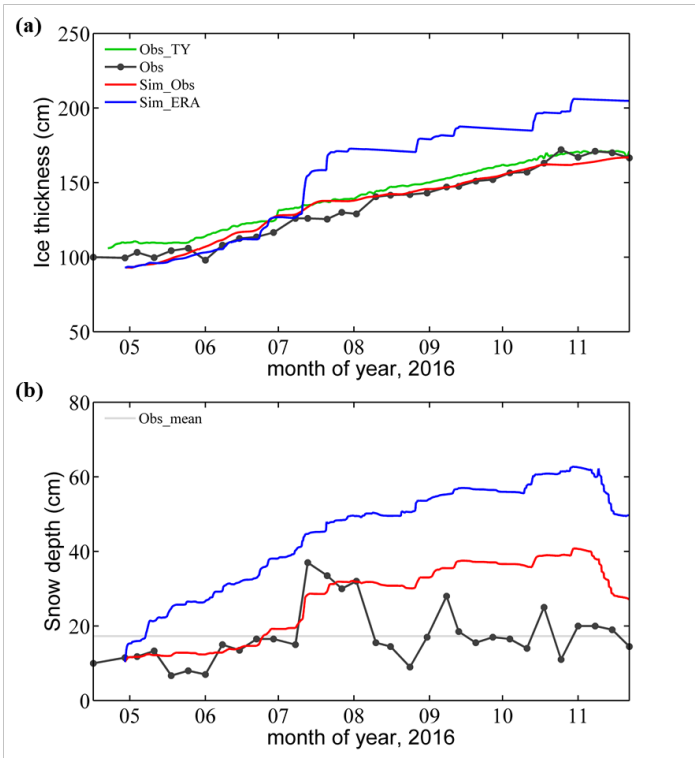

Figure 3 Time series of (a) sea ice thickness and (b) snow depth during the freezing season. Black solid lines with black point show the observations from the drill hole (Obs). In (b) the gray solid line shows the seasonal mean snow depth observation (Obs_mean). Green solid lines show the ice thickness derived from the TY buoy (Obs_TY). Red solid lines show the simulation results under *in situ* atmospheric forcing (Sim_Obs) and blue solid lines are simulation result under ERA5 forcing (Sim_ERA).

3.3 Simulation forced by ERA5 atmospheric variables

When forced by ERA5, the Sim_ERA shows much greater deviations with respect to Obs in ice thickness (Figure 3a). Sim_ERA sea ice thickness is close to the Obs before 11 July with only a small positive bias of about 1 cm. However, from 11 July to November, the mean bias becomes about 33 cm. During this period, a sudden increase in sea ice thickness happens on 11 July. Thereafter, the offset in the sea ice thickness between the Sim_ERA and the Obs remains almost constant.

In contrast to the Sim_ERA sea ice thickness, the Sim_ERA snow depth is much greater than Obs even before 11 July (Figure 3b). Near the extremely large precipitation event (~19 mm day^{-1}) in July 11 (Figure 2b), the Obs snow depth increases from <20 cm to about 40 cm. Although the

precipitation rate from ERA5 is more than 2 times larger as observed on July 11 (~40 mm day^{-1}) the event is almost not visible in the simulated snow depth. The snow depth increase is near linear from about 10 cm at time of model initiation to almost 60 cm at the onset of surface melting in November. For the entire simulation period, the precipitation from ERA5 obviously causes an overestimation in snow depth.

the reasons for the differences between Sim_ERA and Obs are explored in the sensitivity experiments sections below.

3.4 Sensitivity simulations

To find out which atmospheric variables including T_a, P and U_a are the most crucial in the sea ice simulation, a set of sensitivity simulation experiments is conducted, named SEN1. The simulation under the forcing from the *in situ* observed atmospheric variables is the control experiment and named Sim_Obs. In each experiment of SEN1, one atmospheric variable is replaced by the corresponding variable from ERA5 while all others are identical to those of the control experiment. In Table 3, the averaged bias between the simulation and the observation of the outputs (ice thickness and snow depth) or the forcing atmospheric variable, are listed separately.

Table 3 Bias of ice thickness, snow depth and of each forcing variable derived from SEN1. 'All' means using the full set of ERA5 atmospheric forcing

Variable	Bias		Bias ratio (%)
	Ice (cm)	Snow (cm)	Forcing
R_{sd} (W m^{-2})	-0,044	-0.130	9.031
R_{ld} (W m^{-2})	3.050	2.243	-9.672
T_a (K)	0.001	0.029	-0.453
Q_a (10^{-4} kg kg^{-1})	1.099	-1.299	-9.326
P (mm day^{-1})	14.519	17.312	303.509
Θ_a (K)	-0.483	0.407	0.112
ρ_a (kg m^{-3})	0.119	-0.071	-1.592
U_a (m s^{-1})	-0.311	-3.421	50.735
All	16.824	17.882	/

Comparing the individual biases, it turns out that P and R_{ld} from ERA5 contribute to the bias in sea ice thickness most strongly. For snow depth P, U_a and R_{ld} contribute largest. It can also be seen

that sea ice thickness and snow depth are impacted strongly by the biases in R_{ld} and Q_a. In contrast, T_a from ERA5 is close to the *in situ* observation, so the simulated sea ice thickness and snow depth is hardly impacted. The results from SEN1 reveal that the overestimation in P in ERA5 is the major source for the overestimation of sea ice thickness and snow depth and that the overestimation in U_a partly neutralizes the overestimation in snow depth. For convenience, the simulation with only one atmospheric variable (X) replaced by the corresponding ERA5 variable is named SIM_ERA_X.

Compared with Sim_Obs, Sim_ERA_P is overestimating the snow depth since May (Figure 4b) and shows a significant positive bias in sea ice thickness after 11 July (Figure 4a). Before 11 July, the sea ice thickness from Sim_ERA_P was even smaller than from Sim_Obs.

To find out why the snow and sea ice behave differently, we investigate the net heat flux into the ice surface H_N (positive downward):

$$H_N = Rn + Hs + Hl,$$

where Rn, Hs, and Hl are the net surface radiation flux, the sensible heat flux, and the latent heat flux, respectively. All energy fluxes are defined positive downward. Because the simulated snow layer in SIM_ERA_P is much deeper than in SIM_Obs, the difference of H_N reflects the modification of the surface energy flux due to the changed snow layer. From Figure 4d, it can be deduced that the overestimation of snow depth in SIM_ERA_P results in a positive anomaly of H_N before July 11, which hampers the sea ice growth. Later the difference of H_N becomes quite small. The dependence of H_N on the snow depth is significant when the snow layer is shallow (<20 cm in this study). If the snow layer is deep enough its impact on the net surface heat flux ceases.

After July 11, the difference in sea ice thickness between the two simulations increases quickly from ~0 to >40 cm (Figure 4a). We attribute that to flooding with subsequent snow-ice formation (Powell and others, 2005). The continuously deepening snow layer reduces the sea ice freeboard. When there is heavy snow fall, which happens frequently after July 11, the snow load subpresses the sea ice surface below sea level and sea water is flooding onto the sea ice surface causing the overlaying snow to freeze. This snow-ice formation process will form flooding ice (snow-ice thickness) at the sea ice surface and increase the total sea ice thickness rapidly (Figure 4a). The difference (~100 cm) in accumulated flooding ice (Figure 4c) between Sim_Obs (0.8 cm) and Sim_ERA_P (105.5 cm) is greater than the difference (~40 cm) in simulated sea ice thickness (Figure 4a), while the net surface heat flux compares well after July 11 (Figure 4d). The reason for

this difference may be that as the snow-ice process occurs, the increase in sea ice thickness will reduce the heat transfer between the ocean and the atmosphere, and inhibit the basal growth of sea ice in winter (Figure 4e). The flooding induced snow-ice formation happens with a rate larger than 0.5 cm per hour after July 11. The snowfall (Figure 4f) is calculated by precipitation (Figure 2b) and is converted to new snow depth at the top surface using snow density of 330 kg m^{-3} in ICEPACK (Hunke et al., 2019). Comparing Figure 4b with Figure 4f, we find that the change in snow depth (11 cm) is much lower than the accumulated snow fall (57 cm) because of flooding during precipitation event in July.

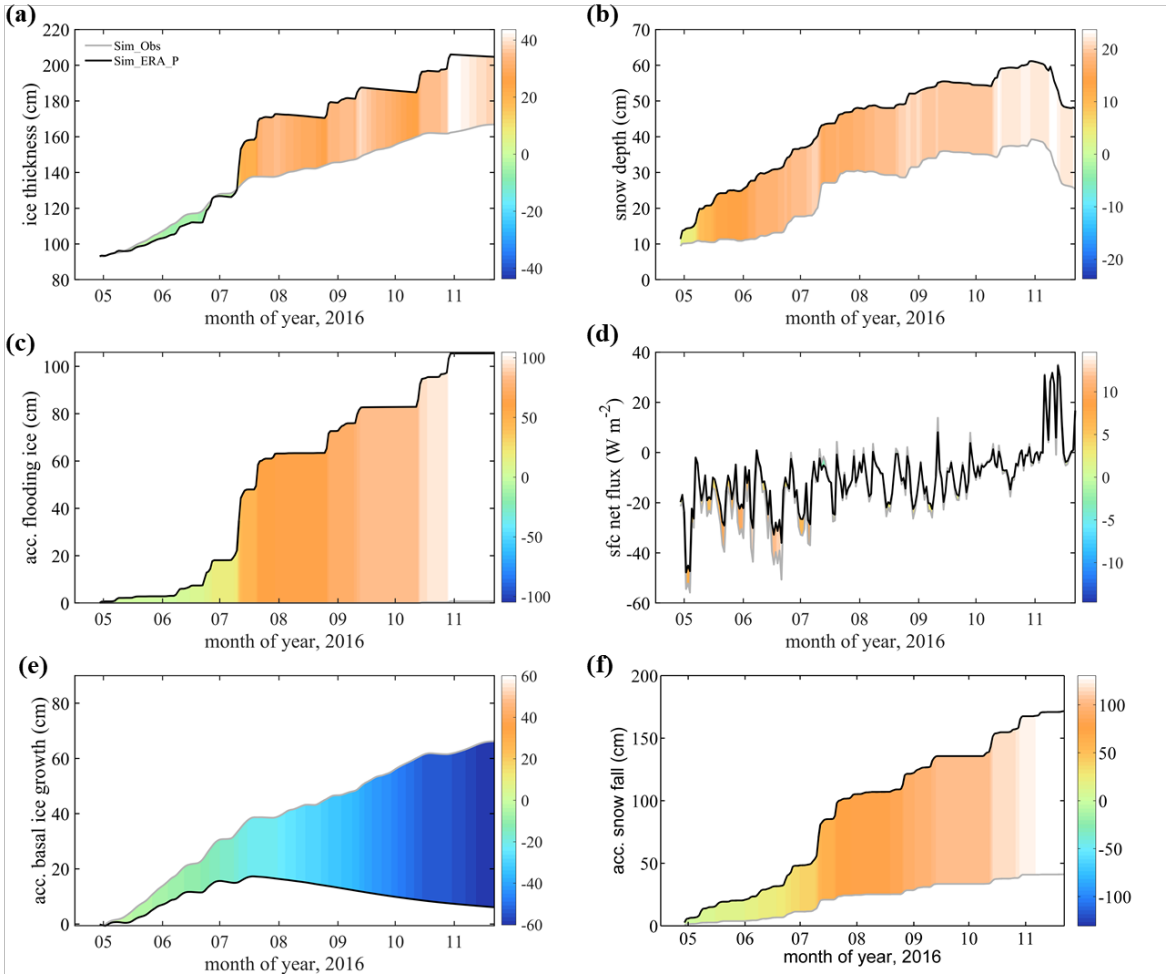

Figure 4 Times series of (a) sea ice thickness, (b) snow depth, (c) accumulated flooding ice, (d) net surface heat flux, (e) accumulated basal ice growth and (f) accumulated snow fall. The gray line represents the simulation using precipitation from observation (Sim_Obs). The black line represents the simulation using precipitation from ERA5 (Sim_ERA_P). The color bar represents their difference (Sim_ERA_P – Sim_Obs).

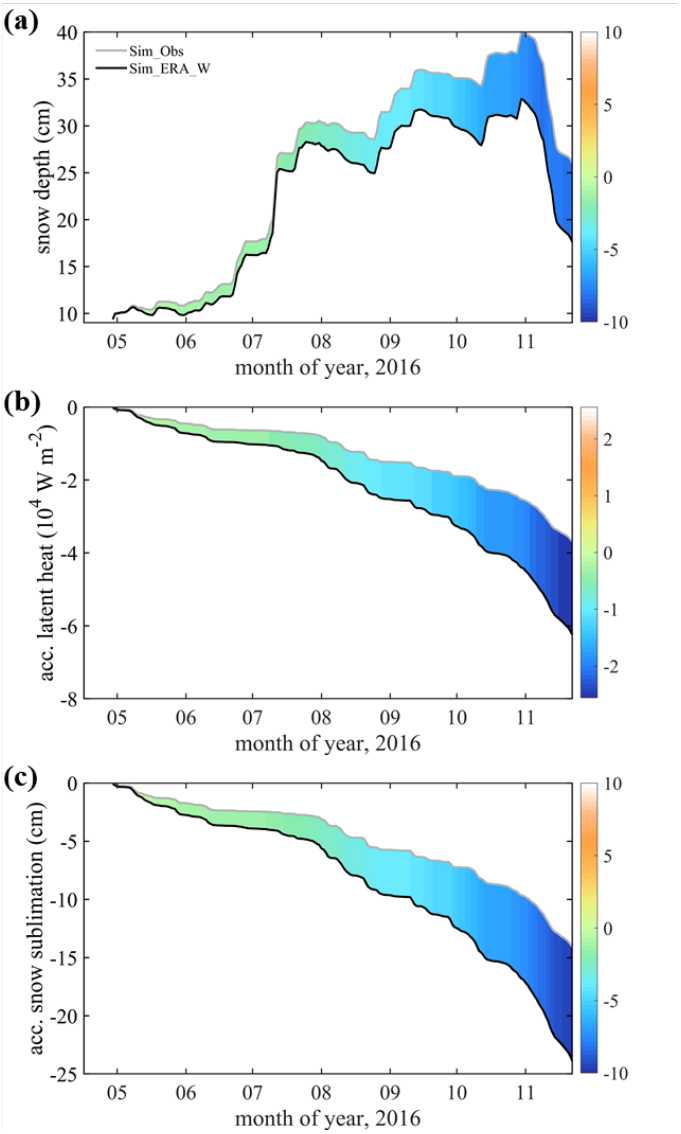

Figure 5 Times series of (a) snow depth, (b) accumulated latent heat flux and (c) accumulated snow sublimation. The gray line represents the simulation using wind from the observation (Sim_Obs). The black line represents the simulation using wind from ERA5 (Sim_ERA_W). The color bar represents their difference (Sim_ERA_W – Sim_Obs).

Although the snow-drift process is currently not implemented in ICEPACK, U_a still affects the snow depth through modifying the surface heat fluxes in the bulk formulations (Fairall et al., 2003). Latent heat changes the snow depth through snow condensation or sublimation process. Compared with Sim_Obs, Sim_ERA_W simulates in the mean a -2.5×10^4 W m^{-2} lower accumulated latent heat (Figure 5b), i.e. a larger sublimation (Figure 5c), and a reduction of about -3.4 cm of the snow depth (Figure 5a). Therefore, when ERA5 is forcing ICEPACK, the overestimation in U_a partly

neutralizes the effect of overestimation in *P* at Zhongshan Station.

3.5 Additional sensitivity simulations on the precipitation bias

The precipitation from ERA5 not only shows the largest deviation compared to the *in situ* observation, but also contributes largest to the bias in the sea ice and snow simulation. To find out how sensitive sea ice and snow are on precipitation, 10 sensitivity experiments are set up, named SEN2 (Figure 6). In the *n*-th experiment, $n \times 10\%$ of the daily difference between *P* from ERA5 and the *in situ* observation is added to the *in situ* observation on that day. This procedure increases the magnitude of the precipitation gradually in the experiments, while the timing of the daily precipitation events remains almost unchanged.

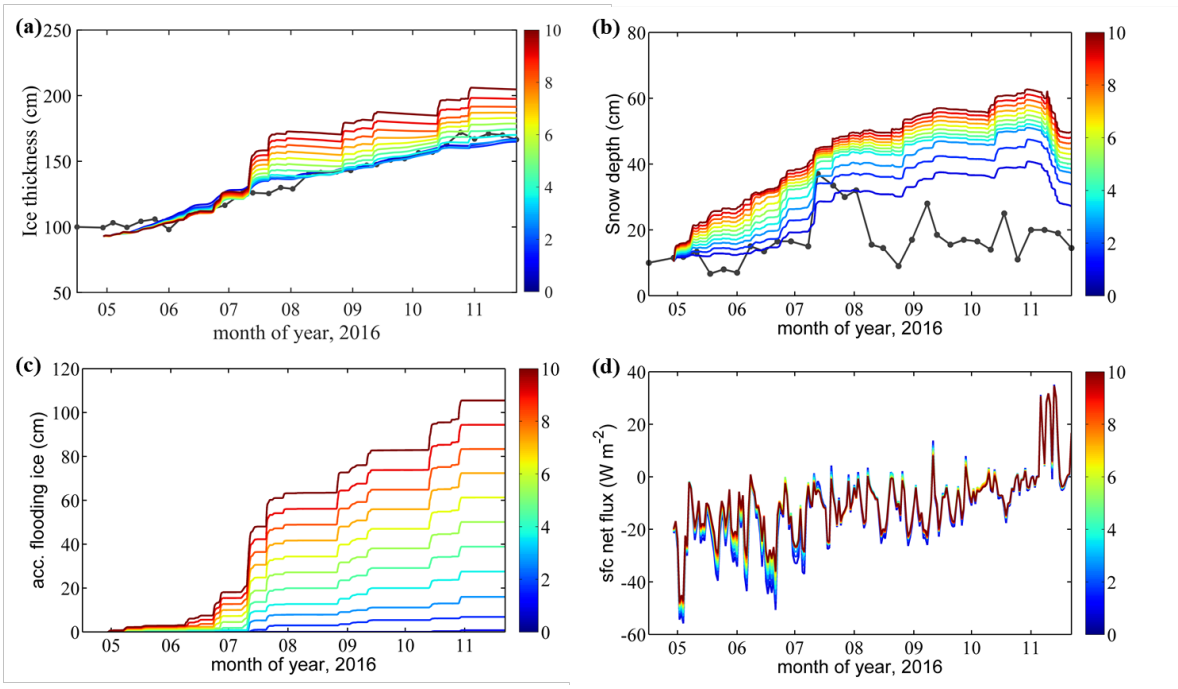

Figure 6 Time series of the simulated (a) sea ice thickness, (b) snow depth, (c) accumulated flooding ice and (d) net surface heat flux in the n experiments of SEN2. The black solid line with black points show the *in situ* observations (Obs). The 11 colored lines denote the 11 sensitivity experiments. When $n = 0$, precipitation is from the *in situ* observation. When $n = 10$, precipitation is from ERA5.

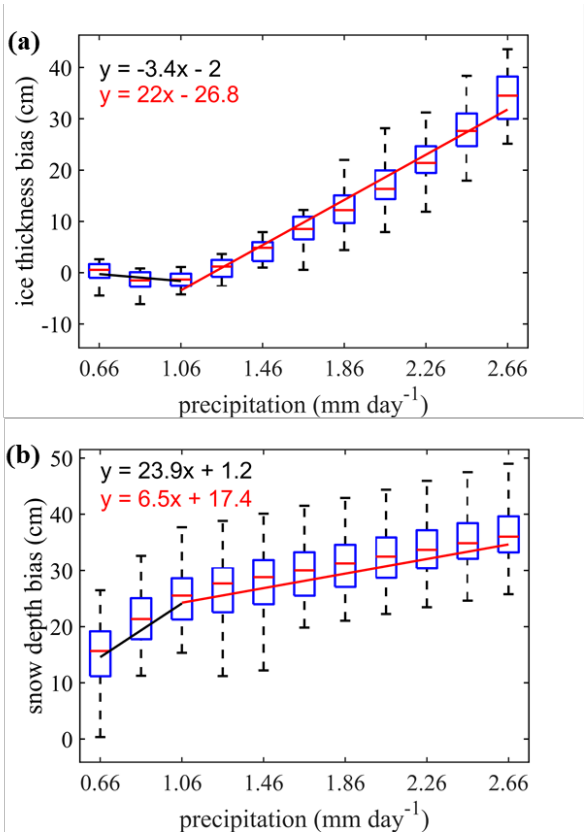

Figure 7 Box plot of simulation bias (simulation minus observation) of (a) sea ice thickness and (b) snow depth over the daily mean precipitation in the different sensitivity experiments (n increases from left to right). On the x-axis, 0.66 mm is referring to the experiment with n=0 (*in situ* precipitation) and 2.66 mm is referring to the n=10 experiment (ERA5 precipitation). Two linear regression lines (black and red) are derived for x <= 1.06 mm and x > 1.06 mm based on the mean of ice thickness and snow depth.

Both, sea ice thickness and snow depth bias exhibit a linear increase with increasing precipitation (Figure 7). The period we calculated the bias between simulations and observations was from 27 July to the end of November. Different start or end dates of this period do not change this result.

The simulation bias of the sea ice thickness is quite small before the precipitation increases by about 1 mm per day (Figure 7). In fact, the simulated sea ice thickness even decreases at a rate of -3.4 cm per 1 mm increase in precipitation. It is because the snow-ice formation is small (Figure 6c) and the stronger isolation of the snow layer (Figure 6d) hampers the sea ice growths. If precipitation is larger than 1 mm day^{-1}, the simulated sea ice thickness quickly increases at a rate of 22 cm/(mm day^{-1}). In contrast, the simulated snow depth deepens rapidly at a rate of 23.9 cm/(mm day^{-1}) when

the enforced precipitation remains small, and at a rate of 6.5 cm when the added precipitation is large. This is because more snow is converted into flooding ice, and the snow-ice formation process strongly overrules the effect of the larger isolation of the thicker snow layer, which promotes the sea ice growth. The snow-ice process is based on Archimedes' Principle. Therefore, the threshold value (1 mm/day^{-1}) is related to the density value of ice, snow and water in model parameterization, and also related to the sea ice thickness and snow depth. If sea ice and snow density, initial snow depth decrease, or sea water density and initial ice thickness increase, the threshold will increase, and vice versa.

These different effects of increases in precipitation on the snow and sea ice growth are illustrated in Figure 8 emphasizing the role of flooding via snow-ice formation. When the snow layer is shallow, increases in precipitation will quickly deepen the snow layer and inhibit the growth of sea ice thickness due to the insulation of snow. The decrease in the surface net heat flux is the dominant factor. While the snow layer is deep and large precipitation is present, the flooding process induces snow-ice formation, and the sea ice grows quickly while the snow depth increases only slowly.

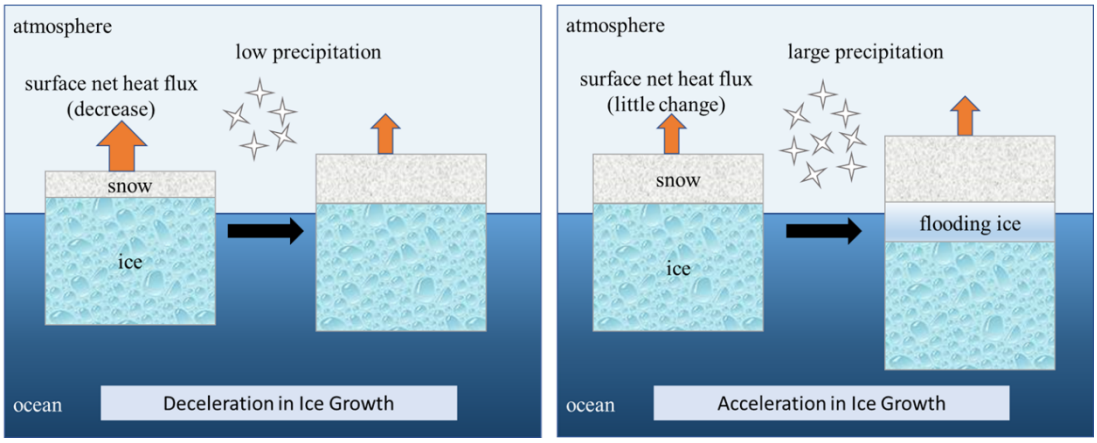

Figure 8 Schematic diagram for (a) low precipitation and (b) large precipitation events illustrating the precipitation effect on sea ice growth. The upward arrows represent surface net heat flux. The white stars represent precipitation. The gray squares represent snow depth. The green squares represent sea ice thickness. The blue squares represent flooding ice.

4 Discussions

Sim_obs is underestimating compared to Obs in November (Figure 3a). The reason might be that superimposed ice was not considered in this study. Superimposed ice usually corresponds to

liquid precipitation or melted snow permeate downward form the ice surface to form a fresh slush layer that refreezes Superimposed ice is present in early autumn when snow starts to melt (Kawamura et al., 1997) and contributes significantly to sea ice growth (up to 20% of mass) (Granskog et al., 2004). The superimposed ice is implemented in ICEPACK via the melt ponds parametrization but that is not used in this study because it would need deformation forcing which is not available at the study area. Therefore, the simulation may underestimate sea ice thickness and overestimate snow depth and we will apply the melt ponds in the follow-up research work.

The snow-ice formation might be overestimated on the landfast sea ice simulation in ICEPACK. Flooding induced snow-ice formation is a very important process in the Antarctic because of thin ice and heavy snowfall (Kawamura et al., 1997). It can make a significant contribution to the total ice mass (12%-36%) and reduces the snow cover by up to 42-70% of the total snow accumulation depending on the season and location (Jeffries et al., 2001). The parameterization of flooding in the ICEPACK is based on Archimedes' Principle for the pack ice. However, the flooding should be much smaller for the landfast sea ice with the same mass of snow cover. Hence, snow-ice formation is probably overestimated on landfast sea ice when using ICEPACK, especially when ERA5 is taken as atmospheric forcing because of its heavy overestimation of precipitation at the study location. Based on observations from a thermistor-chain buoy, a previous study estimated that a slushy layer of 10 cm depth will refreeze within 3 days (Provost et al., 2017). In ICEPACK, snow-ice can form at a fastest rate of 10 cm in 1 day.

Besides the atmospheric forcing, the ocean forcing also plays an important role on sea ice evolution. Heat flux from the ocean boundary layer modifies the sea ice energy balance (Maykut and Untersteiner, 1971). The ocean heat flux is mainly impacted by summer insolation through open leads, thin ice, and melt ponds (Perovich and Maykut, 1990) and upward transfer of heat through vertical turbulent mixing (McPhee et al., 1999). In this study, the oceanic forcing is determined by specifying the ocean temperature and salinity in an ocean mixed layer of 10 m depth. Oceanic observations under sea ice are even more scarce than atmospheric observation over sea ice. Most sea ice models use empirical values or data from CCSM3 to set the ocean boundary values (e.g., Yang et al., 2016b; Turner and Hunke, 2015). However, just as the atmospheric forcing, the marine forcing needs to be evaluated carefully before using (e.g., Uotila et al., 2019).

5 Conclusions

In this work we use the single-column sea ice model ICEPACK forced by the ERA5 atmospheric reanalysis and by atmospheric *in situ* observations to simulate snow depth and sea ice thickness at Zhongshan Station, Antarctic. The main results are:

(1) Using atmospheric variables from *in situ* observations to force ICEPACK simulates the sea ice evolution well, but significantly overestimates the snow depth at Zhongshan Station probably because snow drift process is not implemented in the version of ICEPACK used here.

(2) The average precipitation from ERA5 was about 2 mm day^{-1} greater than observed, hence producing a 14.5 cm excess in sea ice thickness and 17.3 cm more snow depth compared to the simulation forced by observed atmospheric variables. The large bias in precipitation is the main contributor to the simulation bias of sea ice thickness and snow depth between observations and model simulations.

(3) The mean surface wind speed from ERA5 is about 2 m s^{-1} higher than the observation. Directly using surface wind speed alone can reduce the snow bias by 3.4 cm. This is because the increase in latent heat accelerates snow sublimation, but has little effect on the sea ice thickness.

(4) The response of the sea ice thickness was found to depend on the snow depth. When the snow layer is shallow, the snow layer deepens quickly while the sea ice is even growth slowly with increasing precipitation. The change in the surface net heat flux is suggested to be the dominant factor for the change in sea ice thickness. While for a deeper snow layer, because the flooding process induces snow-ice formation, the sea ice grows quickly while the snow depth increases only slowly. This study investigated the ERA5 reanalysis uncertainties and its impact on the sea ice simulation. In our future research, the ocean reanalysis errors and their impact on the sea ice simulation will be addressed as well. Furthermore, because the single-column model only considers sea ice thermodynamics, the full CICE sea ice model will be applied to conduct two dimensional numerical simulations of sea ice for the entire Southern Ocean to assess regional differences and to explore the underlying mechanisms.

Acknowledgments

The authors would like to thank ECMWF for the ERA5 reanalysis data set and the Russian meteorological station Progress II for the precipitation observations. We are grateful to CICE Consortium for sharing ICEPACK and its documentation (https://github.com/CICE-Consortium/Icepack). This study is supported by the National Natural Science Foundation of China (No. 41941009, 41922044), the Guangdong Basic and Applied Basic Research Foundation (No. 2020B1515020025), the Southern Marine Science and Engineering Guangdong Laboratory (Zhuhai) (No. SML2020SP007) and CAS "Light of West China" Program (No. E129030101, Y929641001). PH was supported by AAS grant 4506.

References

Barthélemy, A., Goosse, H., Fichefet, T., and Lecomte, O.: On the sensitivity of Antarctic sea ice model biases to atmospheric forcing uncertainties, Clim. Dynam., 51, 1585-1603, 2018.

Bitz, C. M., Holland, M. M., Weaver, A. J., and Eby, M.: Simulating the ice‐thickness distribution in a coupled climate model, Journal of Geophysical Research: Oceans, 106, 2441-2463, 2001.

Bracegirdle, T. J., and Marshall, G. J.: The reliability of Antarctic tropospheric pressure and temperature in the latest global reanalyses, J. Climate, 25, 7138-7146, 2012.

Briegleb, B. P., and Light, B.: A Delta-Eddington multiple scattering parameterization for solar radiation in the sea ice component of the Community Climate System Model, NCAR Tech. Note NCAR/TN-472+STR, 1-108, 2007.

Bromwich, D. H., Fogt, R. L., Hodges, K. I., and Walsh, J. E.: A tropospheric assessment of the ERA‐40, NCEP, and JRA‐25 global reanalyses in the polar regions, Journal of Geophysical Research: Atmospheres, 112, D10111, 2007.

Chemke, R., and Polvani, L. M.: Using multiple large ensembles to elucidate the discrepancy between the 1979‐2019 modeled and observed Antarctic sea ice trends, Geophys. Res. Lett., 47, e2020G-e88339G, 2020.

Cheng, B., Mäkynen, M., Similä, M., Rontu, L., and Vihma, T.: Modelling snow and ice thickness in the coastal Kara Sea, Russian Arctic, Ann. Glaciol., 54, 105-113, 2013.

Cheng, B., Zhang, Z., Vihma, T., Johansson, M., Bian, L., Li, Z., and Wu, H.: Model experiments on snow and ice thermodynamics in the Arctic Ocean with CHINARE 2003 data, Journal of Geophysical Research: Oceans, 113, C9020, 2008.

Collins, W. D., Bitz, C. M., Blackmon, M. L., Bonan, G. B., Bretherton, C. S., Carton, J. A., Chang, P., Doney, S. C., Hack, J. J., and Henderson, T. B.: The community climate system model version 3 (CCSM3), J. Climate, 19, 2122-2143, 2006.

Fairall, C. W., Bradley, E. F., Hare, J. E., Grachev, A. A., and Edson, J. B.: Bulk parameterization of air–sea fluxes: Updates and verification for the COARE algorithm, J. Climate, 16, 571-591, 2003.

Fréville, H., Brun, E., Picard, G., Tatarinova, N., Arnaud, L., Lanconelli, C., Reijmer, C., and Van den Broeke, M.: Using MODIS land surface temperatures and the Crocus snow model to understand the warm bias of ERA-Interim reanalyses at the surface in Antarctica, The Cryosphere, 8, 1361-1373, 2014.

Gascoin, S., Lhermitte, S., Kinnard, C., Bortels, K., and Liston, G. E.: Wind effects on snow cover in Pascua-Lama, Dry Andes of Chile, Adv. Water Resour., 55, 25-39, 2013.

Granskog, M. A., Leppäranta, M., Kawamura, T., Ehn, J., and Shirasawa, K.: Seasonal development of the properties and composition of landfast sea ice in the Gulf of Finland, the Baltic Sea, Journal of

514 Geophysical Research: Oceans, 109, 10.1029/2003JC001874, 2004.
515 Hao, G., Pirazzini, R., Yang, Q., Tian, Z., and Liu, C.: Spectral albedo of coastal landfast sea ice in Prydz
516 Bay, Antarctica, J. Glaciol., 67, 1-11, 2020.
517 Hao, G., Yang, Q., Zhao, J., Deng, X., Yang, Y., Duan, P., Zhang, L., Li, C., and Cui, L.: Observation
518 and analysis of landfast ice arounding Zhongshan Station, Antarctic in 2016, Haiyang Xuebao, 9, 26-39,
519 2019.
520 Heil, P.: Atmospheric conditions and fast ice at Davis, East Antarctica: A case study, Journal of
521 Geophysical Research: Oceans, 111, C5009, 2006.
522 Heil, P., Allison, I., and Lytle, V. I.: Seasonal and interannual variations of the oceanic heat flux under a
523 landfast Antarctic sea ice cover, Journal of Geophysical Research: Oceans, 101, 25741-25752, 1996.
524 Hersbach, H., Bell, B., Berrisford, P., Hirahara, S., Horányi, A., Muñoz Sabater, J., Nicolas, J., Peubey,
525 C., Radu, R., and Schepers, D.: The ERA5 global reanalysis, Q. J. Roy. Meteor. Soc., 146, 1999-2049,
526 2020.
527 Hersbach, H., and Dee, D.: ERA5 reanalysis is in production, ECMWF Newsletter 147, Reading, UK:
528 ECMWF. [Retrieved from https://www. ecmwf. int/en/newsletter/147/news/era5-reanalysis-production],
529 2016.
530 Hunke, E., Allard, R., Bailey, D. A., Blain, P., Craig, T., Dupont, F., DuVivier, A., Grumbine, R., Hebert,
531 D., Holland, M., Jeffery, N., Lemieux, J., Rasmussen, T., Ribergaard, M., Roberts, A., Turner, M., and
532 Winton, M.: CICE-Consortium/Icepack: Icepack1.1.1, doi:10.5281/zenodo.3251032, 2019.
533 Jeffries, M. O., Krouse, H. R., Hurst-Cushing, B., and Maksym, T.: Snow-ice accretion and snow-cover
534 depletion on Antarctic first-year sea-ice floes, Ann. Glaciol., 33, 51-60, DOI:
535 10.3189/172756401781818266, 2001.
536 Jones, R. W., Renfrew, I. A., Orr, A., Webber, B., Holland, D. M., and Lazzara, M. A.: Evaluation of
537 four global reanalysis products using in situ observations in the Amundsen Sea Embayment, Antarctica,
538 Journal of Geophysical Research: Atmospheres, 121, 6240-6257, 2016.
539 Kawamura, T., Ohshima, K. I., Takizawa, T., and Ushio, S.: Physical, structural, and isotopic
540 characteristics and growth processes of fast sea ice in Lützow-Holm Bay, Antarctica, Journal of
541 Geophysical Research: Oceans, 102, 3345-3355, 10.1029/96JC03206, 1997.
542 Krumpen, T., Birrien, F., Kauker, F., Rackow, T., Albedyll, L. V., Angelopoulos, M., Belter, H. J.,
543 Bessonov, V., Damm, E., and Dethloff, K.: The MOSAiC ice floe: sediment-laden survivor from the
544 Siberian shelf, The Cryosphere, 14, 2173-2187, 2020.
545 Lei, R., Li, Z., Cheng, B., Zhang, Z., and Heil, P.: Annual cycle of landfast sea ice in Prydz Bay, east
546 Antarctica, Journal of Geophysical Research: Oceans, 115, C2006, 2010.
547 Leppäranta, M.: A growth model for black ice, snow ice and snow thickness in subarctic basins,
548 Hydrology Research, 14, 59-70, 1983.
549 Lindsay, R., Wensnahan, M., Schweiger, A., and Zhang, J.: Evaluation of seven different atmospheric
550 reanalysis products in the Arctic, J. Climate, 27, 2588-2606, 2014.
551 Lindsay, R., and Schweiger, A.: Arctic sea ice thickness loss determined using subsurface, aircraft, and
552 satellite observations, The Cryosphere, 9, 269-283, 2015.
553 Liston, G. E., Polashenski, C., Rösel, A., Itkin, P., King, J., Merkouriadi, I., and Haapala, J.: A distributed
554 snow‐evolution model for sea‐ice applications (SnowModel), Journal of Geophysical Research:
555 Oceans, 123, 3786-3810, 2018.
556 Liu, C., Gao, Z., Yang, Q., Han, B., Wang, H., Hao, G., Zhao, J., You, L., Yang, Y., Wang, L., Li, Y.:
557 Observed surface fluxes over sea ice near Antarctic Zhongshan station from April to November in 2016,

Annals of Glaciology, 61(82) ,12-23, 2020.
Massom, R. A., Eicken, H., Hass, C., Jeffries, M. O., Drinkwater, M. R., Sturm, M., Worby, A. P., Wu, X., Lytle, V. I., and Ushio, S.: Snow on Antarctic sea ice, Rev. Geophys., 39, 413-445, 2001.
Massonnet, F., Fichefet, T., Goosse, H., Vancoppenolle, M., Mathiot, P., and König Beatty, C.: On the influence of model physics on simulations of Arctic and Antarctic sea ice, The Cryosphere, 5, 687-699, 2011.
Maykut, G. A., and Untersteiner, N.: Some results from a time-dependent thermodynamic model of sea ice, Journal of Geophysical Research (1896-1977), 76, 1550-1575, 10.1029/JC076i006p01550, 1971.
McPhee, M. G., Kottmeier, C., and Morison, J. H.: Ocean Heat Flux in the Central Weddell Sea during Winter, J. Phys. Oceanogr., 29, 1166-1179, 10.1175/1520-0485(1999)029<1166:OHFITC>2.0.CO;2, 1999.
Merkouriadi, I., Liston, G. E., Graham, R. M., and Granskog, M. A.: Quantifying the potential for snow‐ice formation in the Arctic Ocean, Geophys. Res. Lett., 47, e2019G-e85020G, 2020.
Parkinson, C. L.: A 40-y record reveals gradual Antarctic sea ice increases followed by decreases at rates far exceeding the rates seen in the Arctic, Proceedings of the National Academy of Sciences, 116, 14414-14423, 2019.
Parkinson, C. L., and Cavalieri, D. J.: Antarctic sea ice variability and trends, 1979-2010, The Cryosphere, 6, 871-880, 2012.
Perovich, D. K., and Maykut, G. A.: Solar heating of a stratified ocean in the presence of a static ice cover, Journal of Geophysical Research: Oceans, 95, 18233-18245, 10.1029/JC095iC10p18233, 1990.
Provost, C., Sennéchael, N., Miguet, J., Itkin, P., Rösel, A., Koenig, Z., Villacieros Robineau, N., and Granskog, M. A.: Observations of flooding and snow‐ice formation in a thinner Arctic sea‐ice regime during the N‐ICE2015 campaign: Influence of basal ice melt and storms, Journal of Geophysical Research: Oceans, 122, 7115-7134, 2017.
Schlosser, E., Haumann, F. A., and Raphael, M. N.: Atmospheric influences on the anomalous 2016 Antarctic sea ice decay, The Cryosphere, 12, 1103-1119, 2018.
Stroeve, J. C., Serreze, M. C., Holland, M. M., Kay, J. E., Malanik, J., and Barrett, A. P.: The Arctic’s rapidly shrinking sea ice cover: a research synthesis, Climatic Change, 110, 1005-1027, 2012.
Stuecker, M. F., Bitz, C. M., and Armour, K. C.: Conditions leading to the unprecedented low Antarctic sea ice extent during the 2016 austral spring season, Geophys. Res. Lett., 44, 9008-9019, 2017.
Tetzner, D., Thomas, E., and Allen, C.: A Validation of ERA5 Reanalysis Data in the Southern Antarctic Peninsula—Ellsworth Land Region, and Its Implications for Ice Core Studies, Geosciences, 9, 289, 2019.
Turner, A. K., Hunke, E. C., and Bitz, C. M.: Two modes of sea‐ice gravity drainage: A parameterization for large‐scale modeling, Journal of Geophysical Research: Oceans, 118, 2279-2294, 2013.
Turner, A. K., and Hunke, E. C.: Impacts of a mushy-layer thermodynamic approach in global sea-ice simulations using the CICE sea-ice model, Journal of Geophysical Research: Oceans, 120, 1253-1275, 2015.
Turner, J., Phillips, T., Marshall, G. J., Hosking, J. S., Pope, J. O., Bracegirdle, T. J., and Deb, P.: Unprecedented springtime retreat of Antarctic sea ice in 2016, Geophys. Res. Lett., 44, 6868-6875, 2017.
Uotila, P., Goosse, H., Haines, K., Chevallier, M., Barthélemy, A., Bricaud, C., Carton, J., Fučkar, N., Garric, G., and Iovino, D.: An assessment of ten ocean reanalyses in the polar regions, Clim. Dynam., 52, 1613-1650, 2019.
Vancoppenolle, M., Timmermann, R., Ackley, S. F., Fichefet, T., Goosse, H., Heil, P., Leonard, K. C.,

Lieser, J., Nicolaus, M., and Papakyriakou, T.: Assessment of radiation forcing data sets for large-scale sea ice models in the Southern Ocean, Deep Sea Research Part II: Topical Studies in Oceanography, 58, 1237-1249, 2011.

Vignon, É., Traullé, O., and Berne, A.: On the fine vertical structure of the low troposphere over the coastal margins of East Antarctica, Atmos. Chem. Phys., 19, 4659-4683, 2019.

Wang, C., Graham, R. M., Wang, K., Gerland, S., and Granskog, M. A.: Comparison of ERA5 and ERA-Interim near-surface air temperature, snowfall and precipitation over Arctic sea ice: effects on sea ice thermodynamics and evolution, The Cryosphere, 13, 1661-1679, 2019b.

Wang, G., Hendon, H. H., Arblaster, J. M., Lim, E., Abhik, S., and van Rensch, P.: Compounding tropical and stratospheric forcing of the record low Antarctic sea-ice in 2016, Nat. Commun., 10, 1-9, 2019a.

Wang, Y., Zhou, D., Bunde, A., and Havlin, S.: Testing reanalysis data sets in Antarctica: Trends, persistence properties, and trend significance, Journal of Geophysical Research: Atmospheres, 121, 12-839, 2016.

Yang, Q., Liu, J., Leppäranta, M., Sun, Q., Li, R., Zhang, L., Jung, T., Lei, R., Zhang, Z., and Li, M.: Albedo of coastal landfast sea ice in Prydz Bay, Antarctica: Observations and parameterization, Adv. Atmos. Sci., 33, 535-543, 2016a.

Yang, Y., Zhijun, L., Leppäranta, M., Cheng, B., Shi, L., and Lei, R.: Modelling the thickness of landfast sea ice in Prydz Bay, East Antarctica, Antarct. Sci., 28, 59-70, 2016b.

Zhang, J.: Increasing Antarctic sea ice under warming atmospheric and oceanic conditions, J. Climate, 20, 2515-2529, 2007.

Zhang, J.: Modeling the impact of wind intensification on Antarctic sea ice volume, J. Climate, 27, 202-214, 2014.

Zhao, J., Cheng, B., Yang, Q., Vihma, T., and Zhang, L.: Observations and modelling of first-year ice growth and simultaneous second-year ice ablation in the Prydz Bay, East Antarctica, Ann. Glaciol., 58, 59-67, 2017.

Zhao, J., Cheng, B., Vihma, T., Yang, Q., Hui, F., Zhao, B., Hao, G., Shen, H., and Zhang, L.: Observation and thermodynamic modeling of the influence of snow cover on landfast sea ice thickness in Prydz Bay, East Antarctica, Cold Reg. Sci. Technol., 168, 102869, 2019.